Entanglement-informed construction of variational quantum circuits

Alina Joch[1, 2, *] and Benedikt Fauseweh[1, 3, †]

[1] *Condensed Matter Theory, TU Dortmund University, Otto-Hahn-Straße 4, 44227 Dortmund, Germany*
[2] *Institute for Software Technology, German Aerospace Center (DLR), 51147 Cologne, Germany*
[3] *Institute of Software Technology, German Aerospace Center (DLR), 51147 Cologne, Germany*

(Dated: May 15, 2024)

Variational quantum algorithms are a promising way of efficiently simulating quantum systems with currently developed noisy intermediate scale quantum devices. However, the number of quantum bits and of applied gates still need to be low due to few available quantum bits and errors induced by each gate. Therefore, we use the entanglement information about the system to reduce both. We analyze the ground state energy as well as the entanglement spectra of different systems. We show that impurity models suit well for circuit cutting, a technique to reduce the number of quantum gates and quantum bits in a calculation by dividing the circuit into smaller sub-circuits. In the case of long-range entanglement a singlet initial state can reduce the depth of the quantum circuit compared to the normally used product state. This shows that entanglement-informed construction of variational quantum circuits can streamline variational quantum algorithms allowing for better use of current quantum devices.

I. INTRODUCTION

Since Feynman's idea of using quantum computers to simulate quantum mechanical systems [1], there has been a lot of research in the area of quantum simulation [2–5]. One goal is to find ground state energies of such systems with quantum algorithms designed for the given quantum devices [6–8]. However, one major difficulty is to build large-scale fault-tolerant quantum computers. Currently, only noisy intermediate-scale quantum (NISQ) devices [9] exist making it necessary to reduce the quantum circuit to a small number of gates and used quantum bits (qubits).

In order to still take advantage of these devices, special algorithms are used that fulfill these restrictions [10]. One suggestion is the use of hybrid classical-quantum algorithms, such as variational quantum algorithms (VQAs) [11], where computational tasks are addressed using a combination of classical and quantum computation. The quantum computation of a VQA consists of a parametrized quantum circuit depending on a set of classical parameters, e.g., the rotation angles of single-qubit gates. In a classical computation the next set of these parameters is found by minimizing a cost function. This cost function is designed so that its minima encode the solution of the given optimization problem. With several quantum-classical optimization loops optimized parameters are found.

One kind of VQA is the variational quantum eigensolver (VQE) [11, 12], which is used to efficiently provide an approximation to the ground state energy of many-body quantum systems, potentially offering solutions to problems that are intractable for classical algorithms. The quantum circuit in the VQE algorithm tries to approximate a unitary transformation that rotates a product state into the ground state of a given hamiltonian. The parametrized quantum circuit of the VQE can consist of several layers of the same set of quantum gates. The more layers are used, the higher is the accuracy of the result of the VQE [13]. However, more layers also mean more gates and therefore a higher error. In conlusion, this means that VQA already has advantages compared to other algorithms, but still it is of great interest to find possibilities to further optimize VQA [14, 15].

We will address two approaches based on the given entanglement information about the system to minimize the number of qubits as well as the number of layers opening the way to modeling larger quantum systems with few layers by still obtaining high accuracy:

The first approach is motivated by circuit cutting. This method makes a trade-off between classical and quantum computation [16–18]: The quantum circuit is cut at some points and the different sub-circuits are simulated separately with the quantum computer. The information of the different parts is exchanged classically. Since the classical information exchange is costly, it is only reasonable to use this method, if few cuts are sufficient in order to divide the circuit usefully. However, in systems where this is possible, circuit cutting significantly reduces the number of quantum gates as well as qubits in a calculation, which can further streamline VQE approaches by decreasing the hardware demands and potentially mitigating errors introduced through gate operations [16–18]. Therefore, our goal is to study in which systems it is useful to apply the method. The question that we address is: In which way does the behaviour of the accuracy for different number of layers change in different systems, when changing the number of entangling gates in a given circuit? We will mainly focus on critical phases and only give some comments on the behaviour at gapped phases.

Critical systems and systems with long-range couplings are especially challenging for VQA [19]. In VQE normally

* alina.joch@tu-dortmund.de
† benedikt.fauseweh@tu-dortmund.de

a product state is used as initial state of the parameterized quantum circuit. As a second approach we will investigate whether a singlet state based on the entanglement structure of the given system can decrease the number of layers while still achieving a desired accuracy. In Ref. [20] a similar approach is used to study correlated topological phases showing that an adequate initial state can reduce the number of layers necessary in the quantum circuit.

We will not only use the energy obtained with VQE to analyze the two approaches but also the entanglement spectrum. There has been great interest in the entanglement entropy and spectrum already without looking at quantum computation, e.g. for impurity systems, spin chains and disordered systems [21–23]. Additionally, it is also started to be used to understand the behavior of quantum circuits in VQA [13, 20, 24].

The article is set up as follows. After this Introduction, the studied models are motivated and discussed in Sec. II. Particularly, we present the transverse field Ising model and the XXZ model both with an additional impurity for the first approach. For the second approach, a Heisenberg chain with additional long-range couplings is chosen. Then, Sec. III explains the used methods including a more detailed description of the VQE and the chosen ansätze for the quantum circuit. Subsequently, in Sec. IV A the accuracy of the ground state energy is investigated for the given models and the number of cuts needed to achieve a specific accuracy is determined. In Sec. IV B we look at the entanglement spectrum and the overlap and find good agreement with the results obtained for the energy. Then, in Sec. V we discuss the energy and entanglement spectrum for different parameter values of the Heisenberg chain and values are found for which the singlet initial state gives a better result. In the conclusion VI we argue/ summarize that ...

II. MODELS

A. Approach I: Model for circuit cutting

We will study the behaviour of two quantum spin chains. As we want to find a system that can be properly described by an ansatz that only needs a few cuts to be divided, it is convenient to use a system that has a separate structure itself. Therefore, in each spin chain we add an impurity to the normal model. This is done by applying a magnetic field to the central spin of the chain. By fixing this spin, the left and the right part of the chain can be separated more and more depending on the value of the applied magnetic field.

The first model we investigate is the transverse field Ising model (TFIM). Its hamiltonian is given by

$$H_{\mathrm{TFIM}} = \sum_i \left(-\sigma_i^z \sigma_{i+1}^z + h^x \sigma_i^x\right) + h_0^z \sigma_0^z \,, \qquad (1)$$

where h^x is the disordering magnetic field. The last term describes the impurity at the central spin of the chain. For $|h^x| < 1$, the system is in a ferromagnetic phase with all spins being aligned along the z direction for $|h^x| \to 0$. For $|h^x| > 1$, the system is in a paramagnetic phase. In the limes of $|h^x| \to \infty$ all spins are aligned along the x direction. Between the two phases, at $|h^x| = 1$, is a quantum critical point, where the system gets gapless. The TFIM is described by a conformal field theory with central charge $c = 1/2$.

As comparison we will also study the behaviour of the XXZ model. Its hamiltonian is given by

$$H_{\mathrm{XXZ}} = \sum_i \left(\sigma_i^x \sigma_{i+1}^x + \sigma_i^y \sigma_{i+1}^y + \Delta \sigma_i^z \sigma_{i+1}^z\right) + h_0^z \sigma_0^z \quad (2)$$

with the spin anisotropy Δ. Again, the last term induces the impurity. This model is gapped for $|\Delta| \gg 1$. For $\Delta < -1$, the spins are aligned ferromagnetically, while for $\Delta > 1$, they are aligned anti-ferromagnetically along the z-direction. For $-1^+ \leq \Delta \leq 1$, the system is in a critical phase and is described by a conformal field theory with central charge $c = 1$. When looking at a critical point, we will choose $\Delta = 0.5$ to be far enough from the Heisenberg point as well as the gapped phases.

Both chains are exactly solvable making it possible to compare the results obtained with the VQE with the exact values of the ground state. We will in all cases use open boundary conditions to make a separation of the chain with increasing impurity strength possible.

B. Approach II: Advantages of singlet initial state

To study the influence of an initial singlet state and of different ansatz schemes on the accuracy of VQE depending on the number of layers we use a chain with Heisenberg couplings. Additionally, we add couplings between spins which are several sites apart from each other. This can be described by

$$H_{\mathrm{SL}} = \alpha \sum_i \left(\vec{S}_i \vec{S}_{i+1}\right) + J \sum_{\substack{i=1,\\ j=n-(i-1)}}^{n/2} \left(\vec{S}_i \vec{S}_j\right) \qquad (3)$$

with n being an even total number of spins of the chain. Effectively, this describes a spin ladder mapped to a one dimensional chain. We will mainly focus on the regime $\alpha < J$.

III. METHODS

A. VQE

The quantum circuit of the VQE with finite-depth depending on a set of parameters represents a unitary $U'(\vec{\theta})$. The goal of the VQE is to find the best approximation $U'(\vec{\theta}_{\mathrm{opt}})$ of the exact unitary U that rotates the

initial product state $|0\rangle^{\otimes n}$ into the ground state of a given hamiltonian H of a system with n qubits. For this, we use quantum-classical optimization loops: By applying the circuit with any choice of parameters $\vec{\theta}$ to the initial state we get a trial wave function $|\psi'(\vec{\theta})\rangle = U'(\vec{\theta})|0\rangle^{\otimes n}$. With this trial wave function, we can in a next step calculate our cost function. The cost function to find the ground state of the system is given by the expectation value of the energy depending on the given wave function $E'_{\vec{\theta}} = \langle\psi'(\vec{\theta})|H|\psi'(\vec{\theta})\rangle$. The cost function is minimized with a classical optimization algorithm to find the best parameters $\vec{\theta}_{\text{opt}} = \text{argmin}_{\vec{\theta}} E'_{\vec{\theta}}$. With the optimized parameters we then get the best approximation of the ground state of the hamiltonian $|\psi'(\vec{\theta}_{\text{opt}})\rangle = U'(\vec{\theta}_{\text{opt}})|0\rangle^{\otimes n}$ obtainable with the given quantum circuit.

B. Approach I: Model for circuit cutting

From this, it is already visible that the best approximation we can get depends on the chosen architecture of the quantum circuit. We will use a quantum circuit build from a finite set of gates, i.e., single-qubit rotations and two-qubit controlling gates. We combine those gates to a hardware efficient ansatz: In a first step, we apply a x-rotation and a z-rotation to every qubit. In a next step, we apply R_{zz} gates to neighboring spins but not including the first and the last qubit as we later want to separate the different parts. This forms one layer of the quantum circuit which can be applied several times. We choose the R_{zz} gate instead of the often used $CNOT$ gate to make sure that by applying $m+1$ layers we always get at least the same accuracy as for m layers.

The accuracy of the result for the two given models depending on the number of layers in a given circuit was already studied in Ref. [13]. Here, we want to focus on the influence of different numbers and positions of entangling gates on the accuracy depending on the number of layers. This is done in the context of circuit cutting, i.e., we want to find a circuit which can be divided by a few cuts while still giving a certain accuracy. To divide the circuit discussed so far, we would need one cut in every layer. To reduce this number we have to reduce the number of entangling gates. As in our models we apply an impurity to the central spin, we will vary the number of layers in which gates are applied to this spin/ qubit. As notation we will use $x = [$"layers including gates applied to central spin"$]$. The ansatz of the circuit together with this notation is visualized in Fig. 1.

C. Approach II: Advantages of singlet initial state

In the second approach, we are not interested in changes of the quantum circuit itself but in the influence of changing the initial state on which the quantum gates are applied. Therefore, the quantum circuit stays

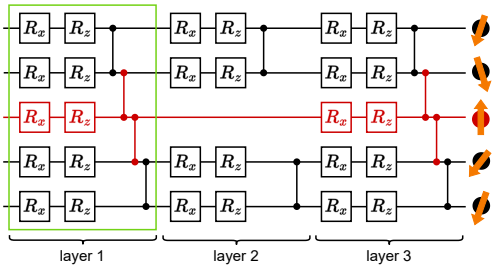

FIG. 1. Variational quantum ansatz used in the simulations depicted exemplarily for five qubits and three layers. One layer is indicated by the green box consisting of a R_x and a R_z rotation applied to each qubit followed by R_{zz} gates. The gates marked in red are only included in the layer if its number is included in x, i.e., here $x = [1, 3]$.

the same (while the optimized parameters of course can be different for different initial states). The chosen circuit is depicted in Fig. 2. The two-qubit gates are again given by R_{zz} gates.

As described before, normally a product state is used as initial state of VQE. Here, we will compare the product state with a singlet initial state. Singlets are built between spins with long-range couplings induced by the second term of Eq. (3). This is visualized in Fig. 2 by dots that have the same color. We will use different number of lightcone layers together with the singlet initial state. Moreover, we look at results for different ansätze built from U4 short gate set and U4 long gate set, also depicted in Fig. 2.

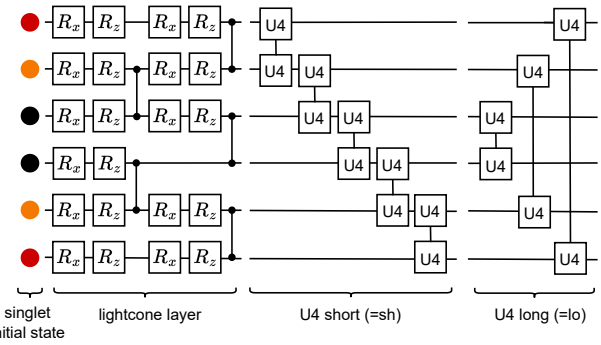

FIG. 2. Variational quantum ansatz used in the simulations of approach II depicted exemplarily for six qubits and two layers. Singlets are built between qubits with the same color of dots.

D. Implementation

We use the programming language Julia for implementation. With the package Yao.jl it is possible to simulate quantum circuits highly efficient [25]. The performance was shown to be much better compared to other tools for simulating quantum computations.

We use the BFGS method implemented in Optim.jl for

the classical optimization step. As initial values for the parameters $\vec{\theta}$ for $m+1$ layers we use the result from m layers and add random numbers close to zero for the additional parameters for the added layer. This makes it possible to reduce the total number of iterations and to increase the precision of the results[14] which is one of the major difficulties here, especially for large numbers of layers. For the second approach, several runs with different random numbers are necessary to make sure that the results are well converged.

To be able to make statements about the accuracy, the exact energy E and exact ground state $|\psi\rangle$ are needed. We calculate this with the eigsolve function from KrylovKit.jl which determines the smallest eigenvalues and its corresponding eigenvectors of a matrix using the Lanzcos algorithm. We will in the next section look at the relative accuracy of the result $\varepsilon_{\text{rel}} = \left(E - E'_{\vec{\theta},\text{opt}}\right)/E$ depending on the number of applied layers.

The calculations are performed with double precision making it in principle possible to achieve relative accuracies of up to -16. When increasing the number of spins and the number of layers the simulation time increases fast. Therefore, up from 11 or 13 spins we let the calculations of the quantum circuit run on GPUs allowing only for single precision which then reduces the possible accuracy of the total calculation. This means that it has to be kept in mind when looking at the following results that the precision of results with high accuracy is decreased.

IV. MODEL FOR CIRCUIT CUTTING

We start to look for a model which can be analyzed with circuit cutting. In a first step, we look at the energy to find a model which can be simulated with a quantum circuit which has a block-like structure. In a second step, we analyze the entanglement entropy and spectrum to get a better understanding of the results obtained in the first step and to make conclusions on how to transfer the results to other models.

A. Energy

In the following, the energy E' gets calculated for different number of layers while varying x and the parameters. The results are compared with the exact result E by looking at the logarithmic value of the relative accuracy $\varepsilon_{\text{rel}} = (E - E')/E$.

We find that for finite length of x the accuracy converges to a plateau in all cases, i.e., gapped and critical phase, with and without impurity, for both models. Moreover, the value of the plateau depends in all cases on the absolute number of entanglements: By adding a layer to x the value of the plateau gets more accurate. This can be seen for both models at the critical point in Fig. 3 and Fig. 4, exemplarily for 9 spins.

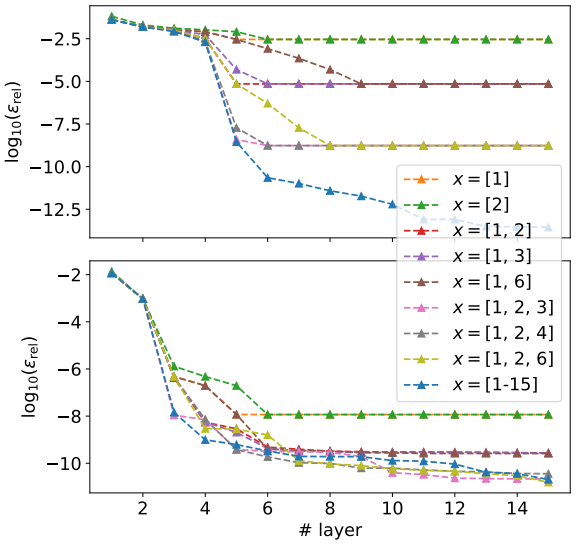

FIG. 3. Accuracy obtained by the VQE for the TFIM model at $h^x = -1.$ without impurity, $h_0^z = 0.$, (top) and with impurity, $h_0^z = -10.$, (bottom) for 9 spins compared to the exact result in a logarithmic plot. Results for different x are shown.

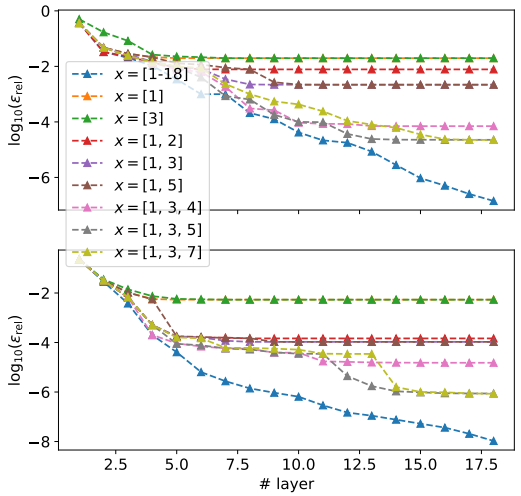

FIG. 4. Accuracy obtained by the VQE for the XXZ model at the critical point without impurity, $h_0^z = 0.$, (top) and with impurity, $h_0^z = -10.$, (bottom) for 9 spins compared to the exact result in a logarithmic plot. Results for different x are shown.

In Fig. 3, it can be seen that the value of the plateau does not depend on the position of entanglement gates but only on the total number. The earlier the entanglement gates are applied, i.e., the smaller the numbers of x, the earlier the value converges to the plateau value.

This is different, however, for the XXZ model as can be seen in Fig. 4. A better result is achieved when the entanglement gates are applied in every second layer than applying it in the first layers while keeping the total number of entanglement gates constant. The same accuracy

is reached if the entanglement gates are applied later, but again more layers are necessary then. These results for the TFIM model and the exact model were also found in the gapped phases.

In critical phases, two regimes have been observed for the convergence [13]: For small numbers of layers the accuracy improves slowly not depending on the system size. Therefore, this regime is called finite-depth regime. After a critical number of layers depending linearly on the system size, a finite-size regime starts. In this regime, the accuracy again improves exponentially. This behaviour can also be seen in our results. However, when comparing the results with and without impurity, one large difference can be seen concerning the transition to exponential improvement of the accuracy, especially for the TFIM model: With impurity the number of layers needed to get exponential improvement is halved. Therefore, we plot the accuracy depending on the number of layers for $x = [\text{all}]$ for changing system size, in Fig. 5 for the TFIM and in Fig. 6 for the XXZ model.

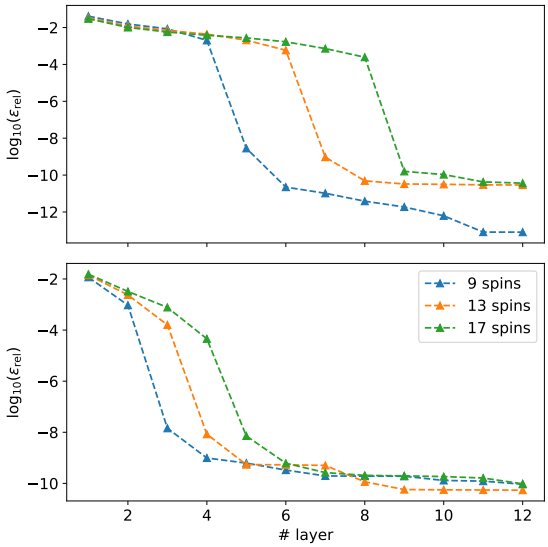

FIG. 5. Accuracy depending on the number of layers for the TFIM model with $x = [\text{all}]$ for varying system size without impurity, $h_0^z = 0.$, (top) and with impurity, $h_0^z = -10.$, (bottom) at the critical point. By including the impurity, the finite-depth regime is halved.

Without impurity we can reproduce the results from Ref. [13]: First, we see a finite-depth regime, where the accuracy only depends on the depth of the circuit but not on the size of the system. Then, after a certain number of layers a finite-size regime is reached, which depends on the system size and where an exponential improvement of the accuracy is achieved (the plateaus at high numbers of layers are formed because of the precision given by the CPUs and GPUs). The separation into these two regimes is an important difference to gapped phases. With impurity we can now see for both models that the finite-depth regime is halved. This behaviour can be explained by the bisection of the chain induced by the impurity.

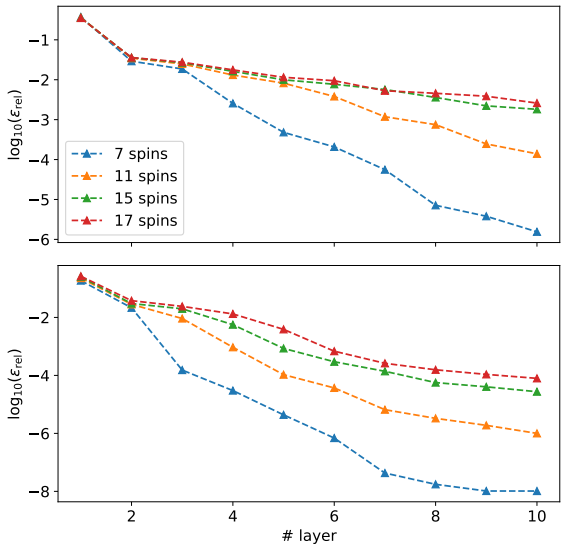

FIG. 6. Accuracy depending on the number of layers for the XXZ model with $x = [\text{all}]$ for varying system size without impurity, $h_0^z = 0.$, (top) and with impurity, $h_0^z = -10.$, (bottom) at the critical point. By including the impurity, the finite-depth regime is halved.

In Fig. 7, the same is visible for $x = [1]$ for the TFIM model. It can be seen that although the finite-size regime, i.e., the exponential behaviour, is reached earlier with impurity, the plateau needs the same amount of layers to be reached as without impurity. For more x and for the XXZ model, due to precision problems it is not clear if the same number of layers is needed to reach the plateau as without impurity but in general the plateau is not reached decisively earlier (often later) as without impurity. In the following step, we choose the value of the plateau as a comparable size, but want to emphasize here that in the case with impurity with less layers, especially for the TFIM, already a considerable improvement of the accuracy can be achieved after the change of regimes. This could be an interesting point when executing the calculation on a real quantum device as less layers correspond to less gates thus possibly the emerging errors are reduced.

We will in a final step look at the plateau values for different number of x (applied in the first layers in case of the TFIM model and in every second layer in case of the XXZ model) for both models with and without impurity for different system sizes.

In Fig. 8, this is shown for the TFIM model for $1x, 2x$ and $3x$, where the number in front of x indicates the number of layers included in x. We can see that by increasing the number of layers in x the accuracy of the result increases for all chain lenghts. Without impurity, the difference of the accuracy for different number x decreases with increasing system size. This is not visible with impurity due to reaching machine precision. What can be seen, however, is that with impurity for a larger system size only one entanglement gate of the central

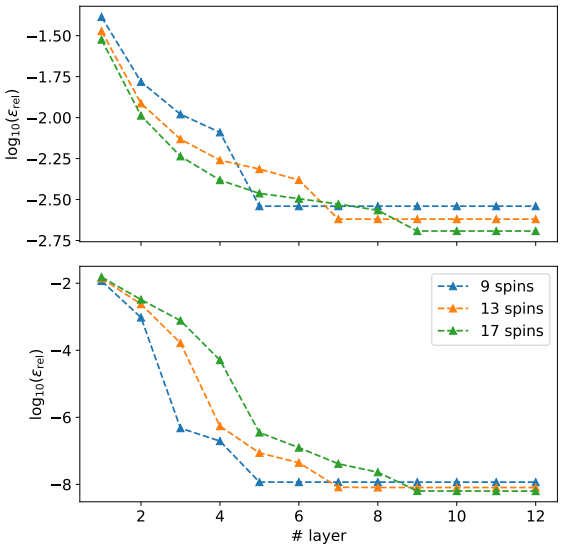

FIG. 7. Accuracy depending on the number of layers for the TFIM model at $h^x = -1.$ with $x = [1]$ for varying system size without impurity, $h_0^z = 0.$, (top) and with impurity, $h_0^z = -10.$, (bottom). By including the impurity, the finite-depth regime is halved but the number of layers to reach the plateau stays the same.

spin is needed to achieve high accuracy and even better one than without impurity with $3x$.

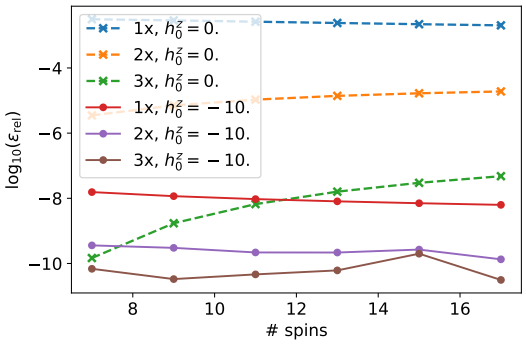

FIG. 8. Logarithmic accuracy obtained with the VQE compared to the exact result for different system sizes number of layers in x for the TFIM model at the critical point. The number of x indicates as well the number of cuts necessary to divide the circuit. Thus, one can read off the number of cuts necessary to achieve a given accuracy.

In Fig. 9 the same is plotted for the XXZ model. Again, with increasing number of layers in x the accuracy of the result increases for all chain lengths. Also the difference of the accuracy for different number x decreases with increasing system size. However, the difference between the accuracy achieved in the model with impurity and without is not as large as for the TFIM model. Averaged about one more set of entanglement gates with the central spin is required without impurity. Moreover, the overall accuracy achieved is worse than for the TFIM model and we can see more fluctuations in the data. In general, for the XXZ model it is harder to achieve a high precision in the minimization process and more iterations are necessary which increases the runtimes. Therefore, only system sizes up to 13 are simulated.

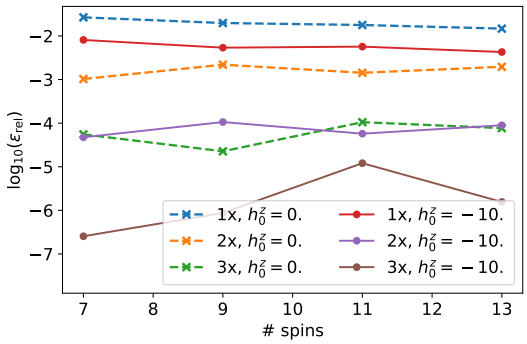

FIG. 9. Logarithmic accuracy obtained with the VQE compared to the exact result for different system sizes number of layers in x for the XXZ model at $\Delta = 0.5$. The number of x indicates as well the number of cuts necessary to divide the circuit. Thus, one can read off the number of cuts necessary to achieve a given accuracy.

With the results from figures 8 and 9 it is possible to read off the number of cuts necessary to achieve a wanted accuracy with a VQE calculation as the number of x corresponds to the number of required cuts. A good choice is the TFIM model with additional impurity as only one cut is necessary to get results in the order of $\log_{10}(\varepsilon_{\text{abs}}) \approx -8.0$.

It is also possible to a priori estimate the needed number of entangling gates depending on impurity strengths when constructing a VQE solution for another system. For that, we will in the next part start with looking at the entanglement entropy compared to the accuracy of the energy for different impurity strengths.

B. Entanglement entropy and spectrum

To calculate the entanglement entropy of the system we need to build the reduced density matrix

$$\rho_{\text{A}} = \text{Tr}_{\text{B}} |\psi\rangle\langle\psi| \tag{4}$$

with A being the left half of the chain and B the right half including the central spin. The entanglement entropy is then given by

$$S = -\,\text{Tr}\left(\rho_{\text{A}} \ln(\rho_{\text{A}})\right) . \tag{5}$$

To better understand the improvemnet of accuracy when adding an impurity we plot the entanglement entropy for different impurity values compared to the accuracy with $1x$ and $2x$ for the TFIM model and compared to $1x$ for the XXZ model. This can be seen in Fig. 10 and Fig. 11, respectively.

It can be seen that with increasing magnetic field the entanglement entropy decreases and the accuracy at the

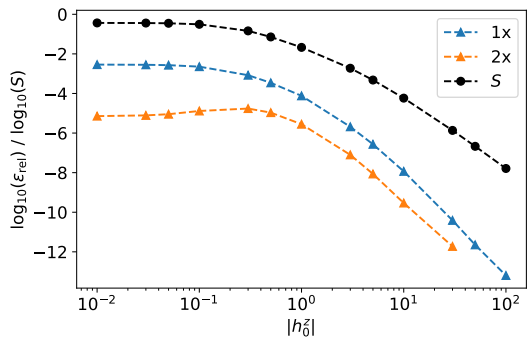

FIG. 10. Logarithmic accuracy obtained with the VQE for $1x$ and $2x$ compared to entanglement entropy for varying impurity strength for the TFIM model with 9 spins.

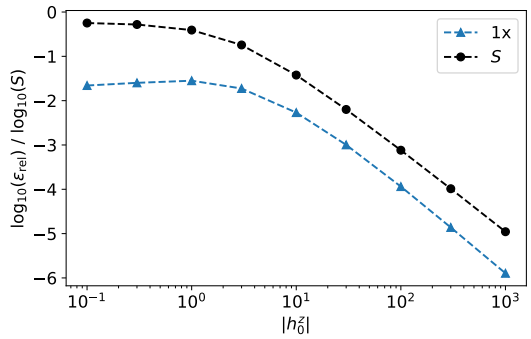

FIG. 11. Logarithmic accuracy obtained with the VQE for $1x$ compared to entanglement entropy for varying impurity strength for the XXZ model with 9 spins.

same time increases. The results in Fig. 11 show why the difference of the plateau values for the XXZ model in the last section was not as large with impurity as for the TFIM model: Much larger impurity values are necessary to significantly reduce the entanglement entropy. To only need one cut an impurity several magnitudes larger than one is necessary in the case of the XXZ model. The reason is that in the XXZ model x and y are the easy plane, and hence the magnetic field in z-direction tends to play a minor role. Therefore, another option is to reduce the coupling strength between two spins in the middle of the chain instead of using an impurity.

In a second step, we will have a look at the energy entanglement spectrum to better understand the improvement of accuracy with increasing number of x. The entanglement spectrum is given by the eigenvalues of the entanglement hamiltonian

$$H_{\rm ent} = -\ln(\rho_{\rm A})\,. \tag{6}$$

In Fig. 12, the entanglement spectrum for the TFIM model with 7 spins without impurity for $x = [1-13]$ is depicted depending on the number of layers. It can be seen that for increasing circuit depth the eigenvalues are captured more precisely. From a number of four layers, all eigenvalues are calculated correctly by the VQE calculation. This fits the transition of the regimes, as for 7 spins without impurity the exponential behaviour is reached after the third layer as can be seen in Fig. 5.

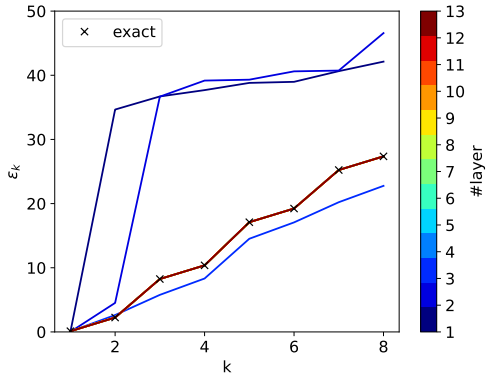

FIG. 12. Eigenvalues ε_k of the entanglement hamiltonian for the TFIM model at the critical point with 7 spins without impurity for $x = [1-13]$ depending on the number of layers compared to the exact solution.

In Fig. 13 the entanglement spectrum is shown for the TFIM model with 9 spins with and without impurity for 13 layers for different x. By increasing the number of layers included in x, more eigenvalues are found with the VQE calculation starting with the smallest eigenvalues. In particular, in the case without impurity the number of correctly found eigenvalues is doubled with each added layer in x. The largest eigenvalues are not calculated correctly even in the case of $x = [\text{all}]$. This is due to the given precision in the calculation as high eigenvalues of the energy entanglement spectrum correspond to extremely small values in the reduced density matrix. One can also see by comparing the exact spectra that including the impurity leads to a separation of the two parts: The first eigenvalue gets smaller, while the following ones get larger. This means that the first value of the reduced density matrix gets closer to one, meaning that the state is less entangled than without impurity.

In Fig. 14 the entanglement spectrum is shown for the XXZ model with 7 spins with and without impurity for 13 layers for different x. Without impurity, there is a degeneracy of the ground state energy meaning that we have a linear combination of potential eigenvectors $|\psi'(\vec{\theta})\rangle$ that can be found by the VQE. Therefore, in this case we use the linear combination of the exact calculation with the smallest overlap with the vector found by the VQE to calculate the exact entanglement spectrum leading to multiple exact spectra. With this, we can find the same results as for the TFIM model: The more layers are included in x, the more accurately the eigenvalues are found starting from the smallest ones. Again, with impurity the difference between the first two eigenvalues gets larger indicating separation of the spin chain. However, the eigenvalues of the XXZ model with impurity are still small compared to those of the TFIM model. This

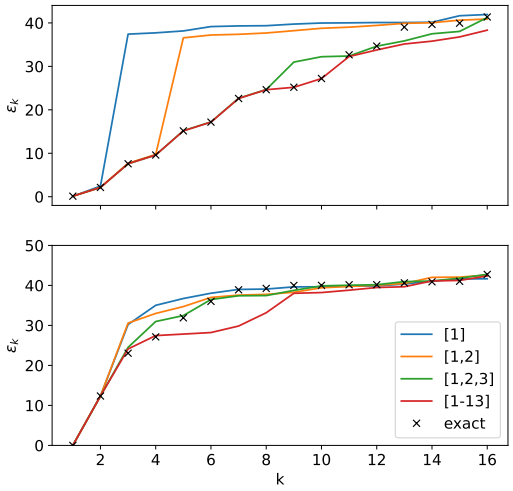

FIG. 13. Eigenvalues ε_k of the entanglement hamiltonian for the TFIM model at $h^x = -1.$ with 9 spins without, $h_0^z = 0.$, (top) and with impurity, $h_0^z = -10.$, (bottom) impurity for 13 layer for different x compared to the exact solution.

means that the XXZ chain is more entangled than the TFIM chain which fits the results of the entanglement entropy.

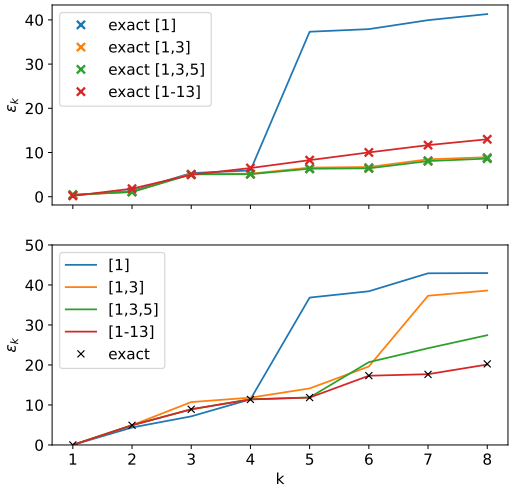

FIG. 14. Eigenvalues ε_k of the entanglement hamiltonian for the XXZ model at $\Delta = 0.5$ with 7 spins withou,t $h_0^z = 0.$, (top) and with impurity, $h_0^z = -10.$, impurity for 13 layer for different x compared to the exact solution.

In a last step, we calculate the overlap between the wave function of the ground state energy obtained with the VQE and with an exact calculation. The results are listed in Tab. I for both models. The values fit well with the results obtained for the energy and the entanglement spectra. One can directly read off which combination of x gives the best results. Deviations can only be found for the XXZ model without impurity for $3x$, where the expected improvement for the choice $x = [1, 3, 5]$ compared to other choices is not visible which is due to the fact that at 13 layers the value is not yet converged to the plateau in that case.

x	TFIM		XXZ	
	$h_0^z = 0.$	$h_0^z = -10.$	$h_0^z = 0.$	$h_0^z = -10.$
1	$5.2 \cdot 10^{-3}$	$6.9 \cdot 10^{-9}$	$3.6 \cdot 10^{-2}$	$1.4 \cdot 10^{-2}$
2	$5.2 \cdot 10^{-3}$	$6.9 \cdot 10^{-9}$	$3.6 \cdot 10^{-2}$	$1.4 \cdot 10^{-2}$
4	$5.2 \cdot 10^{-3}$	$6.9 \cdot 10^{-9}$	$3.6 \cdot 10^{-2}$	$1.4 \cdot 10^{-2}$
1, 2	$3.2 \cdot 10^{-6}$	$6.2 \cdot 10^{-10}$	$4.7 \cdot 10^{-3}$	$1.6 \cdot 10^{-4}$
1, 3	$3.2 \cdot 10^{-6}$	$6.2 \cdot 10^{-10}$	$7.0 \cdot 10^{-4}$	$7.9 \cdot 10^{-5}$
1, 6	$3.2 \cdot 10^{-6}$	$6.3 \cdot 10^{-10}$	$7.0 \cdot 10^{-4}$	$7.9 \cdot 10^{-5}$
1, 2, 3	$9.5 \cdot 10^{-11}$	$3.1 \cdot 10^{-11}$	$6.6 \cdot 10^{-5}$	$1.3 \cdot 10^{-5}$
1, 2, 4	$9.5 \cdot 10^{-11}$	$6.0 \cdot 10^{-11}$	$4.8 \cdot 10^{-5}$	$1.3 \cdot 10^{-5}$
1, 2, 6	$9.5 \cdot 10^{-11}$	$5.5 \cdot 10^{-11}$		
1, 3, 4			$2.8 \cdot 10^{-5}$	$1.0 \cdot 10^{-5}$
1, 3, 5			$3.3 \cdot 10^{-5}$	$1.9 \cdot 10^{-7}$
1 - 13	$2.2 \cdot 10^{-16}$	$1.9 \cdot 10^{-11}$	$1.8 \cdot 10^{-9}$	$1.2 \cdot 10^{-9}$

TABLE I. Overlap of the wave function obtained by the VQE with the exact wave function at a circuit depth of 13 layers and a system size of 7 spins for different x.

V. ADVANTAGES OF SINGLET INITIAL STATE

In this section we will analyze the influence of a singlet initial state and a singlet variational layer on the convergence behaviour of the accuracy as well as of the entanglement spectrum. We look at different regimes of the given model and identify cases in which the singlet state and the singlet variational layer reduce the number of layers necessary to converge to a desired accuracy.

A. Energy

We start to look at Eq. (3) with $J = 1$ and different values $\alpha \ll J$. We calculate the energy with VQE with a product state and with a singlet initial state and plot the relative accuracy as in Sec. IV A. The results are shown in Fig. 15 for 6 spins.

We can see that the smaller α is the better is the result with singlet initial state. This difference is directly present with only one variational layer. Additionally, the results for 8 and for 10 spins are plotted for the first layer with singlet initial state. We can see that there is no dependence on the system size as the accuracy stays the same for different spin chain lengths when looking at the same value of α. This fits with the results of Ref. [20] where it was found for correlated topological phases that with an initial state fitting the given structure of the system only one variational layer is necessary to achieve good results independent of the system size. If we are interested in accuracies of about $10^{-2} - 10^{-6}$ this means

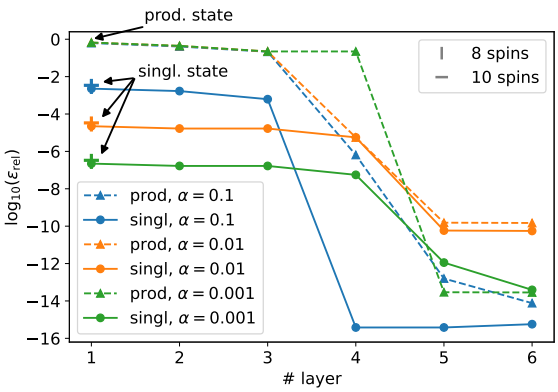

FIG. 15. Accuracy of energy obtained with VQE for 6 spins for different α. Additionally, for the first layer the results for 8 and 10 spins are depicted.

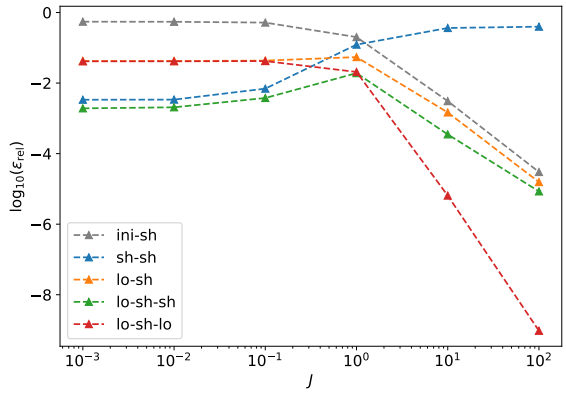

FIG. 16. Comparison of accuracies obtained with different combinations of sh and lo gate sets forming one layer for varying ratio of α and J. Additionally, the results with initial singlet state and one sh gate set are shown in grey for comparison.

that the solution with singlet initial state and one variational layer is already good enough while with a product state several variational layers are necessary to achieve the same accuracy.

However, the accuracy depends directly on the ratio between α and J. For $\alpha \to J$, the accuracy decreases. The number of layers to converge to higher accuracy does not differ significantly between the two initial states, i.e., in Fig. 15 4 to 5 layers are necessary. That is also a problem if $\alpha < J$ but accuracies closer or equal to machine precision are desired. Therefore, it is of interest to find an ansatz with which we can obtain a better accuracy with only one layer. Moreover, with the ansatz chosen so far consisting of R_{zz}-entangling gates we find bad convergence behavior during optimization. For these reasons, we will use a U4-layer ansatz to find the best solution with only one layer.

A first approach is to replace the initial singlet state by a singlet variational layer. We use U4-gates between the spins coupled by J. This then builds one lo gate set as described in Sec. **??**. In Fig. 16, the accuracies obtained with different combinations of the lo gate set with a sh gate set are compared for different ratios of α and J. For comparison, also the results with initial singlet state and one sh gate set are shown in grey.

We can see that for $J > \alpha$ the result with ansätze including a lo gate set is much better than without lo gate set. While the result improves only slightly compared to the singlet initial state a larger improvement is visible for $J < \alpha$. However, the result are still worse than with more sh gate sets in that case and adding one lo gate set only has a small impact. In contrast, adding a second lo gate set to the lo-sh ansatz shows a huge impact. For $J/\alpha = 100.0$ we obtain already accuracies in the order of 10^{-8} with only this one layer. In a next step we check if this result is also valid for larger system sizes.

In Fig. 17, we show the dependence on the system size of the different ansätze for $J/\alpha = 100.0$. The accuracy obtained with the lo-sh-sh ansatz decreases for larger system sizes. This indicates that for small systems the sh gate set is still good enough to capture the long-range interactions which is not longer the case for larger system sizes. However, the other two ansätze including lo gate sets converge to a constant accuracy for larger system sizes. As for the solution with singlet initial state and one variational layer we find a system size independent behavior.

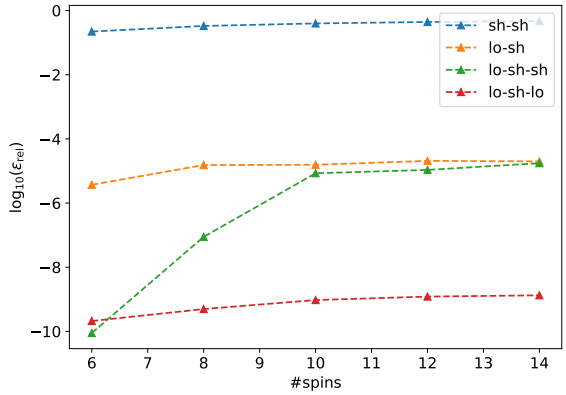

FIG. 17. Dependence on the system size of the different ansätze for $J/\alpha = 100.0$.

This means that we can already identify the lo-sh-lo ansatz as a good choice for $J \ll \alpha$. However, we can see in Fig. 16 that for $J \to \alpha$ the accuracy is worse than 10^{-4} even with the lo-sh-lo ansatz. Therefore, we investigate in a next step whether applying more than one layer of an ansatz including lo gate sets gives an approvement compared to one layer with small number of layers which was not the case for the solutions obtained with an ansatz only consisting of sh gates as visible in Fig. 15. We compare the solution of an sh ansatz with the solution of an lo-sh ansatz for up to 4 layers. The results are depicted in Fig. 18 for $J/\alpha = 3.0$.

When looking at the results of the sh ansatz we find the typical behavior of a critical system with a finite-depth

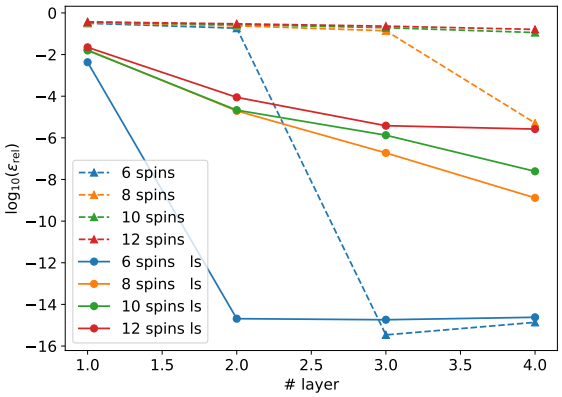

FIG. 18. Accuracy depending on the number of layers for a sh ansatz and a lo-sh ansatz for $J/\alpha = 3.0$ for different system sizes.

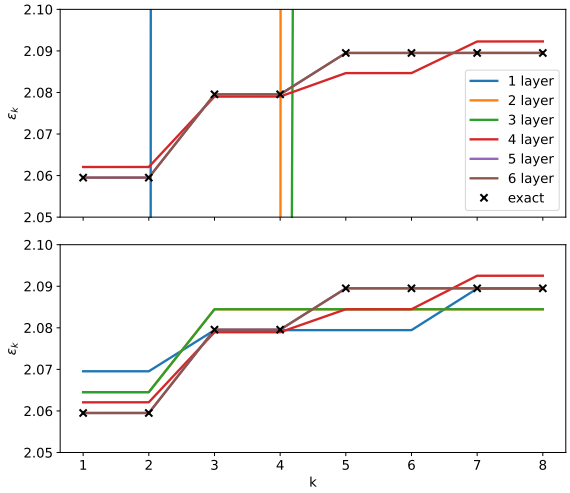

FIG. 19. Entanglement spectrum for $\alpha = 1 \cdot 10^{-2}$ and 6 spins. The upper plot shows the results with product initial state, the lower plot the results with singlet initial state.

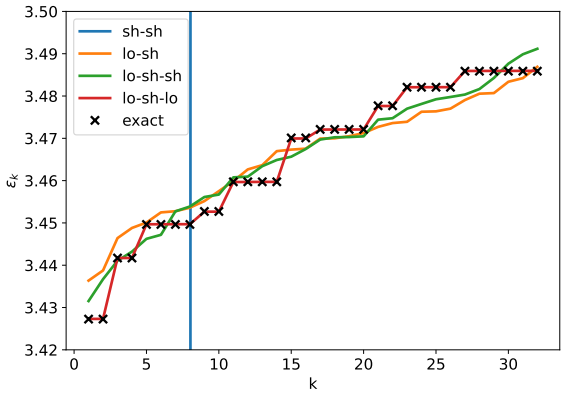

FIG. 20. Entanglement spectrum for the different ansätze compared before for 10 spins and $J = 100.0$.

and a finite-size regime. This means that the larger the system size is the more layers are needed to get an improvement of the accuracy. For the lo-sh layer in general, we also find a finite-depth regime. This is visible for systems sizes larger than 6 spins. The accuracy obtained with VQE only depends on the number of layers. However, this regime has a linear improvement in contrast to the nearly constant behavior in the case of the sh ansatz. Therefore, much better results can be obtained with only few layers. The number of layers necessary to obtain a certain accuracy, i.e., 10^{-8}, depends on the ratio $J/\alpha, J > \alpha$: The larger the ratio, the fewer layers are required.

B. Entanglement spectrum

As before we also look at the entanglement spectrum to get a better understanding of the different convergence behaviors. First, the entanglement spectrum for $\alpha = 1 \cdot 10^{-2}$ and all $J = 1$ of the data showing in Fig. 15 is plotted for 6 spins in Fig. 19.

With singlet initial state the eigenvalues found with VQE are close to the exact ones directly with one layer. With product initial state the eigenvalues are close to the exact ones from the fourth layer. This fits with the results of the accuracy in Fig. 15. One large difference to the behavior in the last section, e.g., in Fig. 12, is that the values are not found starting from the lowest one. It is visible that for small number of layers for small eigenvalues the values are too large and for larger eigenvalues too small in the case of singlet initial state and the other way around in the case of product initial state.

Next, in Fig. 20 we compare the accuracy of the calculated entanglement spectra of the different ansätze in Fig. 16 for $J = 100.0$. When one lo set of gates is included in the ansatz, the results are close to the exact ones. For the lo-sh-lo ansatz, the eigenvalues match the exact ones.

Last, we look at the entanglement spectrum of the data from Fig. 18 for $J/\alpha = 3.0$ for 8 spins. The results are shown in Fig. 21.

We can see a similar behavior as for the singlet initial state. Also we can find the two regimes of critical systems for the sh ansatz as the eigenvalues are found with four layers which matches the change of the regimes. However, with the lo-sh ansatz the eigenvalues are already nearly exact with only two layers. The same is found for 10 spins. This means that although the energy needs more layers to converge, the entanglement spectrum is already captured quite well with only two layers.

VI. CONCLUSIONS

to be done

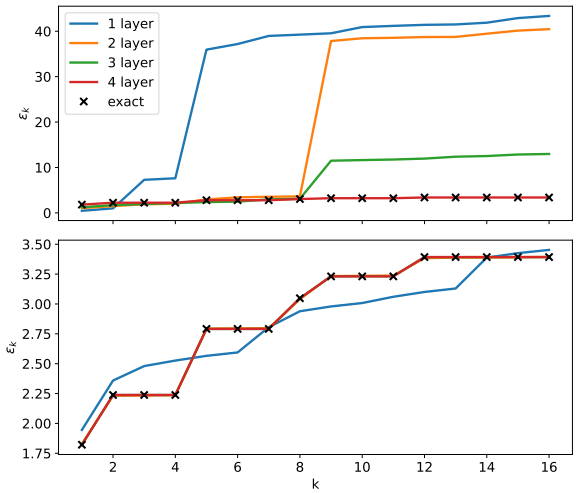

FIG. 21. Entanglement spectrum for the sh ansatz (top) and the lo-sh ansatz (bottom) for $J = 3.0$ for 8 spins.

ACKNOWLEDGMENTS

We thank ... to be done

[1] R. P. Feynman, Simulating physics with computers, International Journal of Theoretical Physics **21**, 467 (1982).

[2] I. Buluta and F. Nori, Quantum simulators, Science **326**, 108 (2009).

[3] K. L. Brown, W. J. Munro, and V. M. Kendon, Using quantum computers for quantum simulation, Entropy **12**, 2268 (2010).

[4] I. M. Georgescu, S. Ashhab, and F. Nori, Quantum simulation, Rev. Mod. Phys. **86**, 153 (2014).

[5] B. Fauseweh, Quantum many-body simulations on digital quantum computers: State-of-the-art and future challenges, Nature Communications **15**, 2123 (2024).

[6] D. S. Abrams and S. Lloyd, Quantum algorithm providing exponential speed increase for finding eigenvalues and eigenvectors, Phys. Rev. Lett. **83**, 5162 (1999).

[7] D. W. Berry, M. Kieferová, A. Scherer, Y. R. Sanders, G. H. Low, N. Wiebe, C. Gidney, and R. Babbush, Improved techniques for preparing eigenstates of fermionic hamiltonians, npj Quantum Information **4**, 10.1038/s41534-018-0071-5 (2018).

[8] Y. Cao, J. Romero, J. P. Olson, M. Degroote, P. D. Johnson, M. Kieferová, I. D. Kivlichan, T. Menke, B. Peropadre, N. P. D. Sawaya, S. Sim, L. Veis, and A. Aspuru-Guzik, Quantum chemistry in the age of quantum computing, Chem. Rev. **119**, 10856–10915 (2019).

[9] J. Preskill, Quantum computing in the NISQ era and beyond, Quantum **2**, 79 (2018).

[10] K. Bharti, A. Cervera-Lierta, T. H. Kyaw, T. Haug, S. Alperin-Lea, A. Anand, M. Degroote, H. Heimonen, J. S. Kottmann, T. Menke, W.-K. Mok, S. Sim, L.-C. Kwek, and A. Aspuru-Guzik, Noisy intermediate-scale quantum algorithms, Rev. Mod. Phys. **94**, 015004 (2022).

[11] M. Cerezo, A. Arrasmith, R. Babbush, S. C. Benjamin, S. Endo, K. Fujii, J. R. McClean, K. Mitarai, X. Yuan, L. Cincio, and P. J. Coles, Variational quantum algorithms, Nature Reviews Physics **3**, 625 (2021).

[12] A. Peruzzo, J. McClean, P. Shadbolt, M.-H. Yung, X.-Q. Zhou, P. J. Love, A. Aspuru-Guzik, and J. L. O'Brien, A variational eigenvalue solver on a photonic quantum processor, Nature Communications **5**, 4213 (2014).

[13] C. Bravo-Prieto, J. Lumbreras-Zarapico, L. Tagliacozzo, and J. I. Latorre, Scaling of variational quantum circuit depth for condensed matter systems, Quantum **4**, 272 (2020).

[14] C. Lyu, V. Montenegro, and A. Bayat, Accelerated variational algorithms for digital quantum simulation of many-body ground states, Quantum **4**, 324 (2020).

[15] N. V. Tkachenko, J. Sud, Y. Zhang, S. Tretiak, P. M. Anisimov, A. T. Arrasmith, P. J. Coles, L. Cincio, and P. A. Dub, Correlation-informed permutation of qubits for reducing ansatz depth in the variational quantum eigensolver, PRX Quantum **2**, 020337 (2021).

[16] S. Bravyi, G. Smith, and J. A. Smolin, Trading classical and quantum computational resources, Physical Review X **6**, 021043 (2016).

[17] Y. Peng, S. Ding, M. Cheng, Q. Hu, J. Yang, F. Wang, M. Xue, Z. Liu, Z. Lin, M. Avdeev, Y. Hou, W. Yang, Y. Zheng, and J. Yang, Magnetic Structure and Metamagnetic Transitions in the van der Waals Antiferromagnet $CrPS_4$, Advanced Materials **32**, 2001200 (2020).

[18] K. Mitarai and K. Fujii, Constructing a virtual two-qubit gate by sampling single-qubit operations, New Journal of Physics **23**, 023021 (2021).

[19] C. Lyu, X. Tang, J. Li, X. Xu, M.-H. Yung, and A. Bayat, Variational quantum simulation of long-range interacting systems, New Journal of Physics **25**, 053022 (2023).

[20] R.-Y. Sun, T. Shirakawa, and S. Yunoki, Efficient variational quantum circuit structure for correlated topological phases, Phys. Rev. B **108**, 075127 (2023).

[21] I. Affleck, N. Laflorencie, and E. S. Sørensen, Entanglement entropy in quantum impurity systems and systems with boundaries, Journal of Physics A: Mathematical and Theoretical **42**, 504009 (2009).

[22] E. Prodan, T. L. Hughes, and B. A. Bernevig, Entanglement spectrum of a disordered topological chern insulator, Phys. Rev. Lett. **105**, 115501 (2010).

[23] G. Torlai, L. Tagliacozzo, and G. D. Chiara, Dynamics of the entanglement spectrum in spin chains, Journal of Statistical Mechanics: Theory and Experiment **2014**, P06001 (2014).

[24] R. Wiersema, C. Zhou, Y. de Sereville, J. F. Carrasquilla, Y. B. Kim, and H. Yuen, Exploring entanglement and optimization within the hamiltonian variational ansatz, PRX Quantum **1**, 020319 (2020).

[25] X.-Z. Luo, J.-G. Liu, P. Zhang, and L. Wang, Yao.jl: Extensible, Efficient Framework for Quantum Algorithm Design, Quantum **4**, 341 (2020).